Electronic Supplementary Material (ESI) for Materials Chemistry Frontiers.

Supporting Information
Modulating the Multiple Intrinsic Properties of Platinum-Iron Alloy Nanowires towards Enhancing Collaborative Electrocatalysis

Fangfang Chang[a], Juncai Wei [a], Qing Zhang [a], Zhichao Jia [a], Yongpeng Liu [a], Lin Yang[a]*, Xiaolei Wang[b] and Zhengyu Bai[a]*

[a] *Collaborative Innovation Center of Henan Province for Green Manufacturing of Fine Chemicals, Key Laboratory of Green Chemical Media and Reactions, Ministry of Education, School of Chemistry and Chemical Engineering, Henan Normal University, Xinxiang, Henan 453007, China. Email:* baizhengyu@htu.edu.cn; yanglin@htu.edu.cn
[b]*Department of Chemical and Materials Engineering, University of Alberta, Edmonton, Alberta T6G 1H9, Canada*

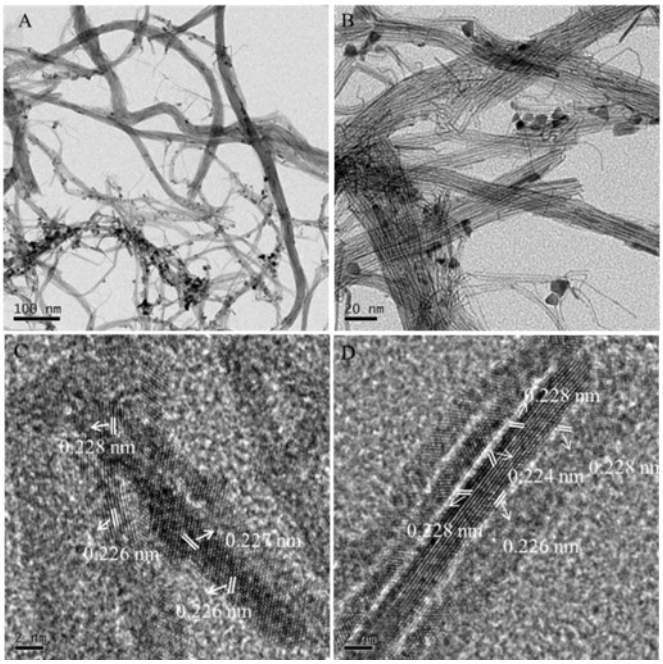

Fig. S1 TEM images (A-B) and HR-TEM images (C-D) of Pt NWs

Table S1. Summary of Particle Sizes and Lattice Constants for PtNi NWs/C Catalysts

Catalysts	NWs size (nm)	Scherrer size (nm)	Lattice parameter (nm)
$Pt_{18}Fe_{82}$/C	20±2.3	19±2.1	0.3713
$Pt_{36}Fe_{64}$/C	2.5±0.4	2.2±0.5	0.3782
$Pt_{62}Fe_{38}$/C	2.1±0.3	2.0±0.3	0.3796
$Pt_{77}Fe_{23}$/C	1.6±0.2	1.8±0.2	0.3813
Pt/C	2.1±0.3	1.9±0.3	0.3920

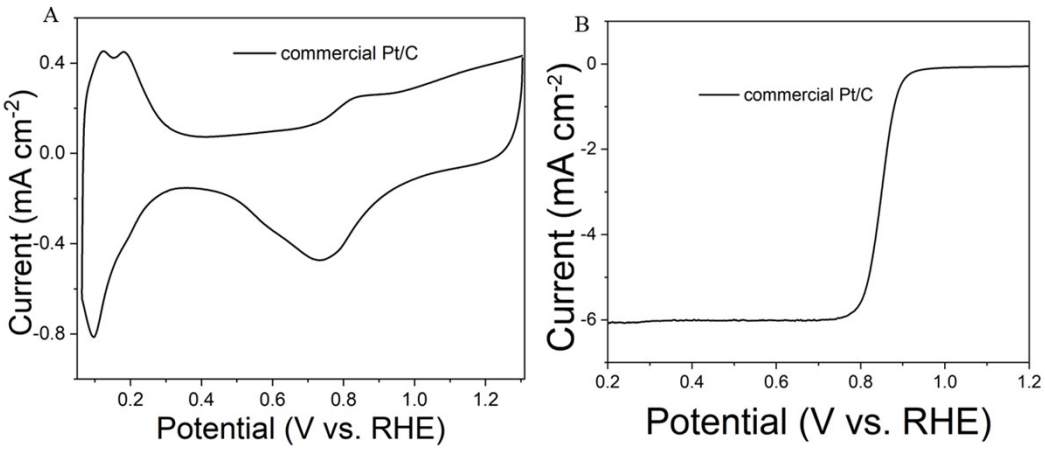

Fig. S2. (A) CV and (B) RDE curves for commercial Pt/C in 0.1 M $HClO_4$ solution saturated with nitrogen (scan rate: 50 mV/s) and oxygen (scan rate: 10 mV/s and rotation speed: 1600 rpm)

Table S2. Summary of physical and ORR data for Pt_nFe_{100-n} NWs/C catalysts

Catalysts	Metal loading (%wt)	ECSA (m^2/g)	Mass activity (A/mg)	Specific activity (mA/cm^2)
$Pt_{18}Fe_{82}/C$	19.00%	24.3	0.40	1.65
$Pt_{36}Fe_{64}/C$	20.00%	35.0	0.60	1.71
$Pt_{62}Fe_{38}/C$	15.00%	69.0	1.03	1.49
$Pt_{77}Fe_{23}/C$	16.00%	76.0	1.68	2.21
Pt NWs/C	15.00%	48.0	0.54	1.13

Table S3. Comparison of ORR activities of various catalysts

Catalyst	Mass activity (A/mg)	Specific activity (mA/cm^2)	Reference
PtFe/Pt-V NWs	1.1	0.88	1
Hollow PtFe	1.01	2.73	2
Ordered Fe_3Pt on nitride	0.67	1.28	3
3D PtFe clusters	1.26	1.51	4
Pt-skin hollow PtFe NPs	0.993	1.35	5
PtFe NWs	0.844	1.53	6
$Pt_{77}Fe_{23}/C$ NWs	**1.68**	**2.21**	**This work**

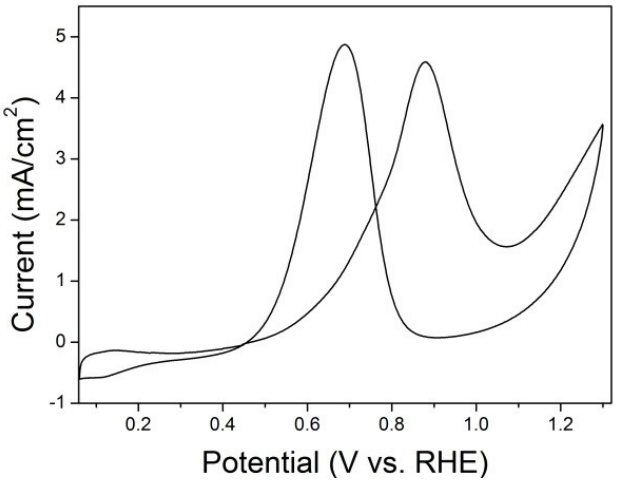

Fig. S3 CV curve of commercial Pt/C in 0.1 M $HClO_4$ + 0.5 M CH_3OH solution purged with N_2 at a scan rate of 50 50 mV/s

Table S4. Summary of physical and MOR data for Pt_nFe_{100-n} NWs/C catalysts

Catalysts	Mass activity (A/mg)	Specific activity (mA/cm^2)
$Pt_{18}Fe_{82}$/C	0.39	1.60
$Pt_{36}Fe_{64}$/C	0.52	1.50
$Pt_{62}Fe_{38}$/C	1.73	2.51
$Pt_{77}Fe_{23}$/C	1.98	2.61
Pt /C	0.47	0.98

Table S5. Comparison of MOR activities of various catalysts

Catalyst	Electrolyte	Mass activity (A/mg)	Specific activity (mA/cm^2)	Reference
PtFe-$Pt_xFe_yCe_zO_j$ Nanohybrids	0.1 M $HClO_4$ + 0.5 M Methanol	0.734	3.28	7
PtFe Intermetallic nanotube	0.5 M H_2SO_4 + 1 M Methanol	0.536	6.16	8
Ga-Pt Intermetallic nanoparticle embed-ded in graphene	0.5 M KOH + 2 M Methanol	0.076	1.48	9
Pt_3Ti/C intermetal-lic nanoparticle	0.1 M $HClO_4$ + 1 M Methanol	0.149	0.03	10
Pt_3V/C intermetallic nanoparticle		0.2	0.038	
Intermetallic Pt_3Zn nanocrystals	1.0 M Methanol	0.25	0.95	11
$Pt_{77}Fe_{23}$/C NWs	**0.1 M $HClO_4$ + 0.5 M Methanol**	**1.98**	**2.61**	**This work**

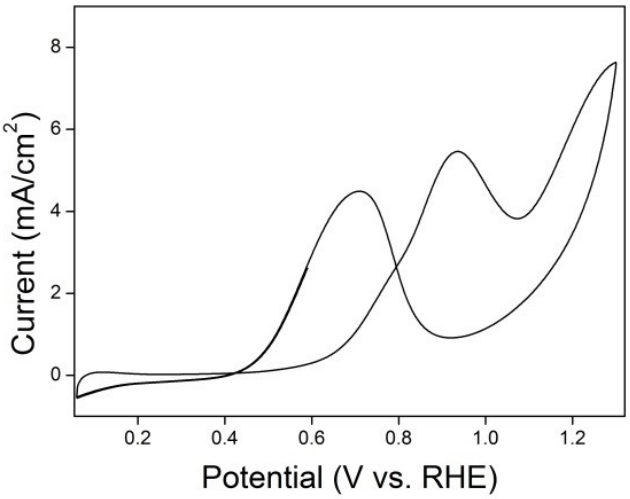

Fig. S4 CV curve of commercial Pt/C in 0.1 M $HClO_4$ + 0.5 M C_2H_5OH solution purged with N_2 at a scan rate of 50 mV/s

Table S6. Summary of physical and EOR data for Pt_nFe_{100-n} NWs/C catalysts

Catalysts	Mass activity (A/mg)	Specific activity (mA/cm^2)
$Pt_{18}Fe_{82}$/C	0.45	1.85
$Pt_{36}Fe_{64}$/C	0.68	1.94
$Pt_{62}Fe_{38}$/C	1.14	1.65
$Pt_{77}Fe_{23}$/C	1.32	1.74
Pt NWs/C	0.32	0.67

Table S7. Comparison of EOR activities of various catalysts

Catalyst	Electrolyte	Mass activity (A/mg)	Specific activity (mA/cm^2)	Reference
$Pt_1Fe_{0.20}Sn_{0.46}$ NWs	0.1 M $HClO_4$ + 0.5 M Ethanol	1.21		12
$PtCu_{2.1}$ NWs	0.1 M $HClO_4$ + 0.2 M Ethanol	1.015	2.16	13
$PtPb_{0.27}$ NWs	0.1 M $HClO_4$ + 0.15 M Ethanol	~ 1.7	~ 0.9	14
PtRhNi/C	0.5 M $HClO_4$ + 1 M Ethanol	0.378		15
RDH PtNi NFs	0.5 M H_2SO_4 + 0.1 M Ethanol	0.98	1.79	16
$Pt_{77}Fe_{23}$/C NWs	**0.1 M $HClO_4$+0.5 M Ethanol**	**1.32**	**1.74**	**This work**

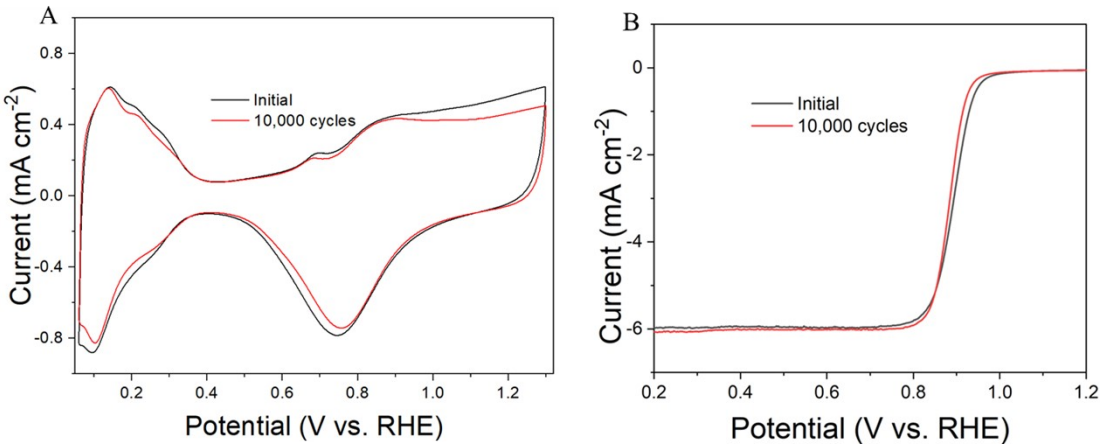

Fig. S5 (A) CV and (B) RDE curves for commercial Pt/C before and after 10,000 potential cycles (sweep rate, 100 mV/s, potential cycle window: 0.6 and 1.1 V) in 0.1 M $HClO_4$ solution saturated with nitrogen and oxygen (scan rate: 10 mV/s and rotation speed: 1600 rpm).

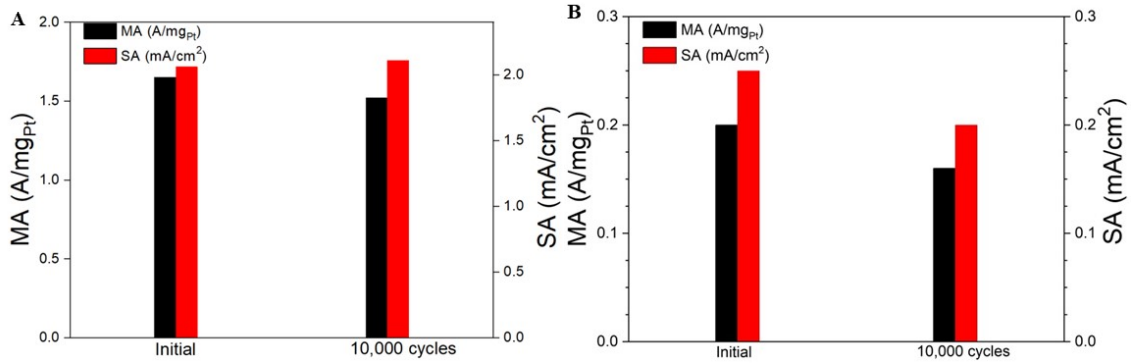

Fig. S6 Mass activity and specific activity data (A) $Pt_{77}Fe_{23}$/C NWs and (B) commercial Pt/C at 0.900 V (vs. RHE) before and after 10,000 cycles.

Table S8. The electron configuration and natural atomic charge of the optimized structure of Pt_xFe_{4-x} (x=1, 2, 3, 4) clusters

cluster	atom No	electron configuration	charge	e-transfer
Pt_4	1Pt	$6S^{0.57}5d^{9.41}6p^{0.08}$	0.00	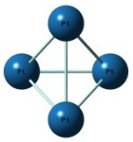
	2Pt	$6S^{0.057}5d^{9.41}6p^{0.08}$	0.00	
	3Pt	$6S^{0.057}5d^{9.41}6p^{0.08}$	0.00	
	4Pt	$6S^{0.057}5d^{9.41}6p^{0.08}$	0.00	
Pt_3Fe_1	1Fe	$4S^{0.44}3d^{6.86}4p^{0.18}$	0.450	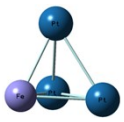
	2Pt	$6S^{0.72}5d^{9.37}6p^{0.09}$	-0.154	
	3Pt	$6S^{0.71}5d^{9.38}6p^{0.09}$	-0.148	
	4Pt	$6S^{0.71}5d^{9.38}6p^{0.09}$	-0.148	
Pt_2Fe_2	1Fe	$4S^{0.61}3d^{6.89}4p^{0.31}$	0.087	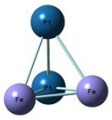
	2Pt	$6S^{0.87}5d^{9.23}6p^{0.11}$	-0.183	
	3Pt	$6S^{0.87}5d^{9.23}6p^{0.11}$	-0.183	
	4Fe	$4S^{0.57}3d^{7.04}4p^{0.12}5p^{0.07}$	0.279	
Pt_1Fe_3	1Fe	$4S^{0.65}3d^{7.14}4p^{0.08}4d^{0.01}5p^{0.14}$	0.111	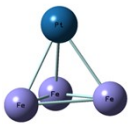
	2Pt	$6S^{1.06}5d^{9.31}6p^{0.07}$	-0.287	
	3Fe	$4S^{0.56}3d^{7.02}4p^{0.09}5p^{0.12}$	0.088	
	4Fe	$4S^{0.56}3d^{7.02}4p^{0.09}5p^{0.12}$	0.088	

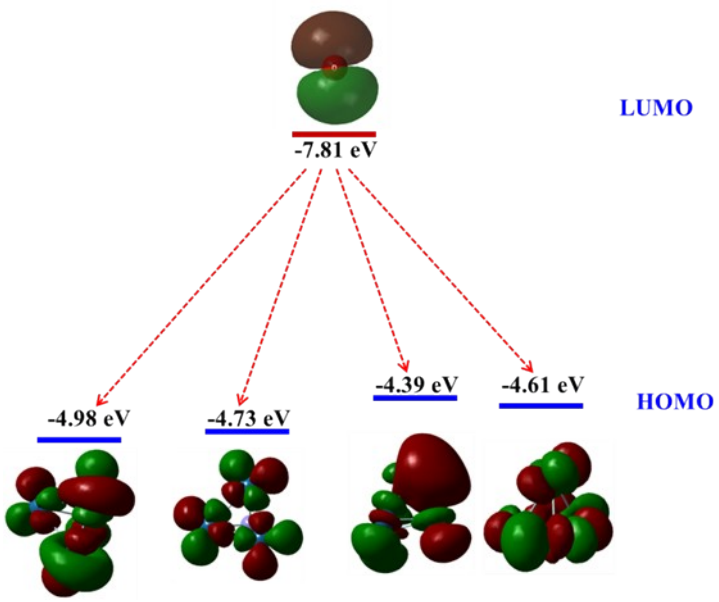

Fig. S7 Frontier molecular orbitals and the energy of LUMO of O atom and HOMO of Pt_xFe_{4-x} (x = 4, 3, 2, 1) clusters

Table S9. Structure and binding energy ((eV) for Pt_xFe_{10-x} (x=2, 4, 6, 8, 10) clusters

Pt_2Fe_8	Pt_4Fe_6	Pt_6Fe_4	Pt_8Fe_2	Pt_{10}
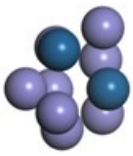	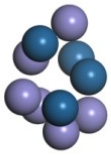	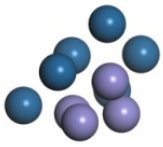	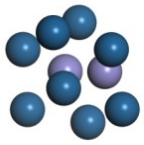	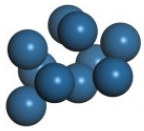
-4.54	-3.96	-2.79	-2.24	-2.20

Table S10. Structure and adsorption energy (eV) for O Pt_xFe_{10-x} (x=2, 4, 6, 8, 10) clusters

	Pt_2Fe_8	Pt_4Fe_6	Pt_6Fe_4	Pt_8Fe_2	Pt_{10}
	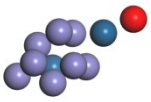	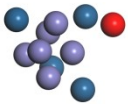	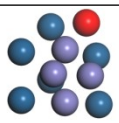	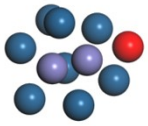	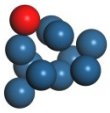
O	-0.18	-0.27	-5.07	-4.99	-4.53

Table S11. Structure and adsorption energy (eV) for OOH Pt_xFe_{10-x} (x=2, 4, 6, 8, 10) clusters

	Pt_2Fe_8	Pt_4Fe_6	Pt_6Fe_4	Pt_8Fe_2	Pt_{10}
	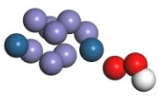	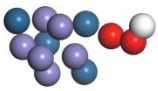	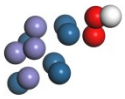	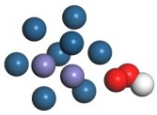	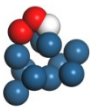
OOH	-1.38	-0.785	-5.74	-2.21	-1.59

Table S12. Structure and adsorption energy (eV) for OH Pt_xFe_{10-x} (x=2, 4, 6, 8, 10) clusters

	Pt_2Fe_8	Pt_4Fe_6	Pt_6Fe_4	Pt_8Fe_2	Pt_{10}
	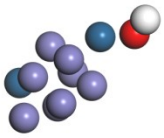	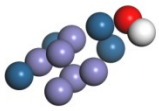	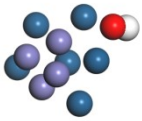	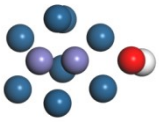	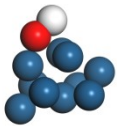
OH	-2.65	-1.32	-2.98	-3.02	-2.41

Table S13. Structure and adsorption energy (eV) for CO Pt_xFe_{10-x} (x=2, 4, 6, 8, 10) clusters

	Pt_2Fe_8	Pt_4Fe_6	Pt_6Fe_4	Pt_8Fe_2	Pt_{10}
	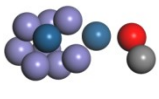	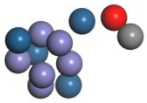	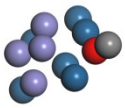	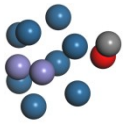	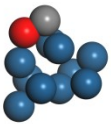
CO	-0.18	-0.27	-5.07	-4.99	-4.53

Table S14. The correction of zero point energy and entropy of the adsorbed and gaseous species.

	ZPE(eV)	TS(eV)
*OOH	0.35	0
*O	0.05	0
*OH	0.31	0.01
H_2O	0.56	0.67
H_2	0.27	0.41

References:

1 Y. H. Shi, W. Yang, W. B. Gong, X. N. Wang, Y. R. Zhou, X. F. Shen, Y. L. Wu, J. T. Di, D. S. Zhang, Q. W. Li, Interconnected surface-vacancy-rich PtFe nanowires for efficient oxygen reduction, *J. Mater. Chem. A.*, 2021, **9**, 12845-12852.

2 Z. J. Yang, L. Shang, X. Y. Xiong, R. Shi, G. I. N. Waterhouse, T. R. Zhang, Hollow PtFe alloy nanoparticles derived from Pt-Fe_3O_4 dimers through a silica-protection reduction strategy as efficient oxygen reduction electrocatalysts, *Chem-Eur. J.*, 2020, **26**, 4090-4096.

3 Q. B. Liu, L. Du, G. T. Fu, Z. M. Cui, Y. T. Li, D. Dang, X. Gao, Q. Zheng, J. B. Goodenough, Structurally ordered Fe_3Pt nanoparticles on robust nitride support as a high performance catalyst for the oxygen reduction reaction, *Adv. Energy Mater.*, 2019, **9**, 1803040.

4 F. Lin, Y. J. Sun, J. P. Lai, K. Wang, Y. H. Tang, Y. G. Chao, Y. Yang, J. R. Feng, F. Lv, P. Zhou, M. H. Huang, S. J. Guo, 3D PtFe clusters with cube-in-cube structure enhance oxygen reduction catalysis and electrochemical sensing, *Small Methods*, 2018, **2,** 1800073.

5 Q. M. Wang, S. G. Chen, F. Shi, K. Chen, Y. Nie, Y. Wang, R. Wu, J. Li, Y. Zhang, W. Ding, Y. Li, L. Li, Z. D. Wei, Structural evolution of solid Pt nanoparticles to a hollow PtFe alloy with a Pt-skin surface via space-confined pyrolysis and the nanoscale kirkendall effect, *Adv. Mater.*, 2016, **28**, 10673-10678.

6 S. J. Guo, D. G. Li, H. Y. Zhu, S. Zhang, N. M. Markovic, V. R. Stamenkovic, S. H. Sun, FePt and CoPt nanowires as efficient catalysts for the oxygen reduction reaction, *Angew. Chem. Int. Ed*., 2013, **52**, 3465-3468.
7 J. G. Ma, X. Tong, J. M. Wang, G. X. Zhang, Y. P. Lv, Y. C. Zhu, S. H. Sun, Y. C. Yang, Y. J. Song, Rare-earth metal oxide hybridized PtFe nanocrystals synthesized via microfluidic process for enhanced electrochemical catalytic performance, *Electrochim*. *Acta*, 2019, **299**, 80-88.
8 X. B. Zhang, S. J. Tian, W. J. Yu, B. Q. Lu, T. Y. Shen, L. Xu, D. M. Sun, S. L. Zhang, Y. W. Tang, Nanotube-shaped PtFe intermetallics: controlled synthesis, crystal structure, and improved electrocatalytic activities, *CrystEngCom*m, 2018, **20**, 4277-4282.
9 V. B. Kumar, J. Sanetuntikul, P. Ganesan, Z. Porat, S. Shanmugam, A. Gedanken, Sonochemical formation of Ga-Pt intermetallic nanoparticles embedded in graphene and its potential use as an electrocatalyst, *Electrochim*. Acta, 2016, **190**, 659-667.
10 Z. M. Cui, H. Chen, M. T. Zhao, D. Marshall, Y. C. Yu, H. Abruña, F. J. DiSalvo, Synthesis of structurally ordered Pt_3Ti and Pt_3V nanoparticles as methanol oxidation catalysts, *J. Am. Chem. Soc*., 2014, **136**, 10206-10209.
11 Y. J. Kang, J. B. Pyo, X. C. Ye, T. R. Gordon, C. B. Murray, Synthesis, shape control, and methanol electro-oxidation properties of Pt-Zn alloy and Pt_3Zn intermetallic nanocrystals, *ACS Nano*, 2012, **6**, 5642-5647.
12 C. Wang, H. Xu, F. Gao, Y. P. Zhang, T. X. Song, C. Q. Wang, H. Y. Shang, X. Zhu, Y. K. Du, High-density surface protuberances endow ternary PtFeSn nanowires with high catalytic performance for efficient alcohol electro-oxidation, *Nanoscale*, 2019, **11**, 18176-18182.
13 N. Zhang, L. Z. Bu, S. J. Guo, J. Guo, X. Q. Huang, Screw thread-like platinum-copper nanowires bounded with high-index facets for efficient electrocatalysis, *Nano Lett*., 2016, **16**, 5037-5043.
14 N. Zhang, S. J. Guo, X. Zhu, J. Guo, X. Q. Huang, Hierarchical Pt/Pt_xPb core/shell nanowires as efficient catalysts for electrooxidation of liquid fuels, *Chem. Mater*., 2016, **28**, 4447–4452.
15 N. Erini, S. Rudi, V. Beermann, P. Krause, R. Z. Yang, Y. H. Huang, P. Strasser, Exceptional activity of a Pt-Rh-Ni ternary nanostructured catalyst for the electrochemical oxidation of ethanol, *ChemElectroChem*, 2015, **2**, 903-908.
16 J. B. Ding, L. Z. Bu, S. J. Guo, Z. P. Zhao, E. B. Zhu, Y, Huang, X. Q. Huang, Morphology and phase controlled construction of Pt-Ni nanostructures for efficient electrocatalysis, *Nano Lett*., 2016, **16**, 2762–2767.